International Journal of Thermal Sciences 111 (2017) 310–320

Contents lists available at ScienceDirect

International Journal of Thermal Sciences

journal homepage: www.elsevier.com/locate/ijts

Natural convection of Al_2O_3-water nanofluid in an inclined cavity using Buongiorno's two-phase model

Saber Yekani Motlagh*, Hosseinali Soltanipour

Department of Mechanical Engineering, Urmia University of Technology (UUT), P.O. Box: 57166-419, Urmia, Iran

ARTICLE INFO

Article history:
Received 22 January 2016
Received in revised form
2 May 2016
Accepted 9 August 2016

Keywords:
Inclined cavity
Natural convection
Nanofluid
Thermophoresis
Brownian
Buongiorno model

ABSTRACT

In the present study, natural convection of Al_2O_3–water nanofluid and nano-particles local distribution inside a tilted square enclosure has been investigated using non-homogenous two-phase Buongiorno's model. The left and right vertical walls of cavity are kept at constant temperatures T_h and T_c, respectively, while the other walls are thermally insulated. Using the finite volume method and the SIMPLE algorithm, the governing equations have been discretized. Simulations have been carried out for different inclination angle ($0^\circ \leq \theta \leq 60^\circ$), Rayleigh number ($10^2 \leq Ra \leq 10^6$) as well as particle average volume fraction (φ) ranging from 0.01 to 0.04. Results show that at low Rayleigh numbers regardless of particle volume fraction, with increasing the inclination angle the average Nusselt number (Nu_{Ave}) and heat transfer enhancement percentage remains almost constant. On the other hand, for high Rayleigh numbers Nu_{Ave} rises and then reduces with inclination angle whereas, heat transfer enhancement percent continuously increases with increasing inclination angle. It is also observed that for all inclination angles and at low Rayleigh numbers, the particle distribution is fairly non-uniform while, at high Ra numbers particles have nearly uniform distribution.

1. Introduction

Because of wide applications of the natural convection, it becomes one of the major topics of research in the last two centuries. These applications occur in industrial and technological applications such as crystal growth, electronic cooling, oil extraction, solar collectors and etc.

Researchers and engineers are extensively seeking to find new ways to respond to industrial demands in the area of advanced thermal sciences. Maxwell's idea of suspension metallic millimeter- or micrometer-sized particles to enhance the thermal conductivity of fluid is well-known [1]. However, such particles cannot be used in micro-systems and micro-devices because of serious problems such as abrasion and clogging. However, modern nanotechnology provides great opportunities to produce materials with the average size of 100 nm or less. These particles can be well-dispersed in conventional heat transfer fluids such as water, ethylene-glycol (EG), and oil to produce a new kind of heat transfer fluid called nanofluids [2]. Miniaturization and thermal management of engineering systems strongly depend on the thermal behavior improvement of working fluids. Nanofluids, as a novel heat transfer fluids, can play an important role in improving the thermal efficiency of engineering devices such as heat exchangers and cooling systems. Thus, numerous investigations have been dedicated to estimate nanofluid thermal properties such as thermal conductivity and viscosity. Results showed that the thermal conductivity of nanofluids, in general, is higher than that of the conventional fluids that are currently used in different thermal devices. Several authors have measured thermal conductivity of nanofluids with different nanoparticle concentrations, mean diameters, materials, and different base fluids. All findings confirm that thermal conductivity of nanofluid is superior to that of base fluid. For example, the thermal conductivity of Al_2O_3/water and TiO_2/water nanofluids with 4.3 vol% is approximately 32% and 11% higher than that of the base liquid, respectively [3].

From numerical point of view, there are two different methods for simulation of flow and heat transfer of nanofluids, namely single-phase and two-phase. In single phase models, it is assumed that the fluid and particles are in thermal equilibrium and move with the same velocity [4,5]. In fact, the effect of particles existence is considered only in effective properties of nanofluids. However, experimental studies show that the validity of the single-phase

* Corresponding author.
E-mail addresses: s.yekani@uut.ac.ir, syekani@yahoo.com (S.Y. Motlagh).

http://dx.doi.org/10.1016/j.ijthermalsci.2016.08.022
1290-0729/

model for nanofluids is somewhat questionable [6]. However, in the two phase models, effect of Brownian motion, thermophoresis and other interactions between carrier fluid and nano-particles are taken into account [7,8]. Homogenous model is one of the single-phase models in which effective properties of nanofluid is applied in the continuity, momentum and energy equations. Therefore, more complex and nonhomogeneous methods such as two-phase mixture models were successfully developed and employed in order to consider slip velocity between the base fluid and particles [9–16].

Buongiorno [9] developed a non-homogeneous equilibrium model by considering the effect of the Brownian, diffusion and thermophoresis. He reported the seven slip mechanisms in nanofluids: inertia, Brownian, diffusion, thermophoresis, diffusiophoresis, Magnus effect, fluid drainage and gravitational settling and concluded that in the absence of turbulence, the Brownian and thermophoresis are the most important effects. In the recent years, a number of investigations have been conducted based on the transport equations derived by Buongiorno. For example, Corcione et al. [10] reported natural convection of nanofluids inside a differentially heated cavity using Buongiorno's model and concluded that the two phase mixture method is more accurate than the single-phase model. A similar study has been conducted by Pakravan and Yaghoubi [12] and Sheikhzadeh et al. [13] to investigate the effects of Brownian diffusion and thermophoresis. Tzou [17,18] investigated the Benárd instability of a quiescent nanofluid between two parallel walls. A numerical study was presented by Garoosi et al. [19] using Buongiorno's model. They analyzed natural and mixed convection heat transfer of a nanofluid (Al_2O_3-water) in a laterally heated square cavity. They observed that at low Rayleigh and high Richardson numbers, the particle distribution is fairly non-uniform while at high Rayleigh and low Richardson numbers particle distribution remains almost uniform for free and mixed convection cases, respectively. For more information see the recent published review papers about single-phase and two-phase treatments of convective heat transfer enhancement with nanofluids [20–22].

Sheremet et al. [23,24] investigated the nanofluid flow and heat transfer in porous cavities using Buongiorno's model. In another work, Sheremet and Pop [25] employed Buongiorno's model to analyze the mixed convection of nanofluid in a lid-driven cavity. The effects of important parameters such as Reynolds, Grashof, Prandtl and Lewis numbers on flow pattern and heat transfer were explored.

Laminar natural convection of nanofluids has been extensively studied in the differentially heated enclosures. But very few works have been performed concerning inclined enclosures. Some researchers have used single-phase or homogenous models to study heat transfer and fluid flow in nanofluids in inclined geometries [26–30]. It was found that in a differentially heated inclined enclosure, the heat transfer rate increases as the inclination angle increases up to an optimum inclination angle (45° for $Ra = 10^4$, 30° for $Ra = 10^5$ and 10^6), beyond which the heat transfer rate decreases [27,29,30]. Aminossadati and Ghasemi [25] studied heat transfer characteristics in an inclined square cavity with and without a central solid block. The inclination had no effect on heat transfer rate at low Rayleigh numbers. On the other hand, at high Rayleigh numbers, with a central block, inclination enhanced heat transfer rate. Recently, Ahmed et al. [31] used the two-phase lattice Boltzmann method (LBM) for the simulation of natural convection in inclined square cavity filled with Al_2O_3-water. Their results showed that thermophoresis has a considerable effect on heat transfer augmentation in laminar natural convection and the optimal inclination angle depends on e Ra number.

This research intends to explore the nano-particles local distribution and the rate of heat transfer of natural convection in an inclined cavity using Buongiorno's model. The effects of Rayleigh number ($10^2 \leq Ra \leq 10^6$), volume fraction ($0 \leq \varphi_{Ave} \leq 0.04$) and inclination angle ($0^\circ \leq \theta \leq 60^\circ$) are investigated. To the best of our knowledge, this study is the first one which used two-phase (inhomogeneous) Buongiorno's model to investigate the effect of inclination angle on nano particle distribution and natural convection of Al_2O_3-water nanofluid in a square cavity.

2. Mathematical modeling

2.1. Problem statement

The schematic of considered problem in the present investigation is shown in Fig. 1. A two-dimensional square cavity with an inclination angle (θ) and height of H is filled with Al_2O_3 -water nanofluid. The top and bottom walls are thermally insulated whereas two vertical walls are at constant but different temperatures T_h and T_c, respectively. As shown, the gravity force acts in the vertical direction.

2.2. Governing equations and boundary conditions

The flow is assumed to be 2D, steady, incompressible and laminar. Nanoparticles are assumed to have uniform shape and size and in thermal equilibrium with the base fluid. The density variation with the temperature in body force term is considered to be linear based on the Boussinesq's model. Moreover, dissipation and pressure work are ignored in the present study. Under the above assumptions the governing equations of continuity, momentum, energy and volume fraction are as follows [9]:

Continuity equation:

$$\nabla \cdot \boldsymbol{V} = 0 \tag{1}$$

Momentum equation:

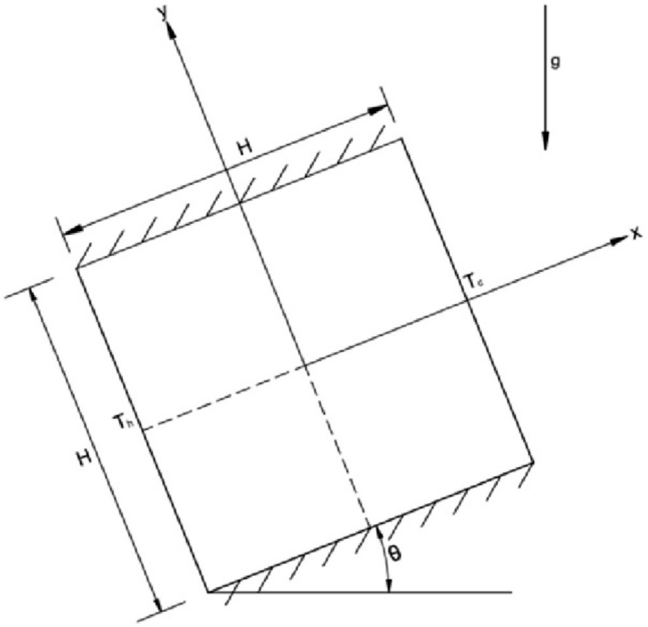

Fig. 1. Geometry of an inclined cavity.

$$\rho_{nf}\boldsymbol{V}\cdot\nabla\boldsymbol{V} = -\nabla p + \nabla\cdot\left(\mu_{nf}\nabla\boldsymbol{V}\right) + (\rho\beta)_{nf}(T - T_c)\boldsymbol{g} \tag{2}$$

where $\boldsymbol{V}$ is the velocity vector and $\boldsymbol{g}$ is the gravitational acceleration vector i.e., $\boldsymbol{g} = -gsin(\theta)\,\vec{i} - gcos(\theta)\,\vec{j}$.

In the above equations ρ_{nf}, μ_{nf} and β_{nf} denote the density, the effective dynamic viscosity and thermal expansion coefficient of nanofluid, respectively; T and p denote temperature and pressure.

Energy equation:

$$(\rho C_p)_{nf}\boldsymbol{V}\cdot\nabla T = \nabla\cdot\left(k_{nf}\nabla T\right) - C_{p,p}\boldsymbol{J_p}\cdot\nabla T \tag{3}$$

Volume fraction equation:

$$\boldsymbol{V}\cdot\nabla\varphi = -\frac{1}{\rho_p}\nabla\cdot\left(\boldsymbol{J_p}\right) \tag{4}$$

where in Equations (3) and (4) k_{nf}, C_{pnf}, $C_{p,p}$ and ρ_p are nanofluid thermal conductivity, nanofluid heat capacity, particle heat capacity and particle density, respectively; φ is the local volume fraction of nanoparticles and $\boldsymbol{J_p}$ is the nanoparticles mass flux. Based on Buongiorno's model nanoparticles mass flux can be written as:

$$\boldsymbol{J_p} = \boldsymbol{J_{p,B}} + \boldsymbol{J_{p,T}} \tag{5}$$

$\boldsymbol{J_{p,B}}$ and $\boldsymbol{J_{p,T}}$ on right hand side of Equation (5) are mass flux due to Brownian motion and thermophoresis effect, respectively.

$\boldsymbol{J_{p,B}}$ is the drift flux due to the Brownian motion defined as [9]:

$$\boldsymbol{J_{p,B}} = -\rho_p D_B\nabla\varphi \tag{6}$$

where the Brownian diffusion coefficient, D_B, is given by the Einsteine-Stokes's equation:

$$D_B = \frac{K_B T}{3\pi\mu_f d_p} \tag{7}$$

$\boldsymbol{J_{p,T}}$ is drift flux due to thermophoretic effects which can be defined as:

$$\boldsymbol{J_{p,T}} = -\rho_p D_T\frac{\nabla T}{T} \tag{8}$$

where D_T is thermophoresis coefficient which can be approximated as [33]:

$$D_T = \lambda\cdot\frac{\mu_f}{\rho_f}\varphi \tag{9}$$

In Equation (9), λ is a constant defined as $\lambda = 0.26k_f/k_f{+}k_p$

Substitution of Equations (6) and (8) into Equation (4), the closed form of volume fraction equation would be as:

$$\rho_p\boldsymbol{V}\cdot\nabla\varphi = \nabla\cdot\left(\rho_p D_B\nabla\varphi\right) + \nabla\cdot\left(\rho_p D_T\frac{\overrightarrow{\nabla T}}{T}\right) \tag{10}$$

By considering no-slip condition and zero mass flux of nanoparticles at the walls, the boundary conditions for Equations (1)–(3) and (10) would be as follows [12,13]:

$$\begin{aligned}
&\boldsymbol{V} = 0,\ \nabla T\cdot\boldsymbol{n} = \nabla\varphi\cdot\boldsymbol{n} = 0 \text{ on the top and bottom walls}\\
&\boldsymbol{V} = 0,\ T = T_h \text{ and } \nabla\varphi\cdot\boldsymbol{n} = -\frac{D_T}{D_B}\nabla T\cdot\boldsymbol{n} \text{ on the left wall}\\
&\boldsymbol{V} = 0,\ T = T_c \text{ and } \nabla\varphi\cdot\boldsymbol{n} = -\frac{D_T}{D_B}\nabla T\cdot\boldsymbol{n} \text{ on the right wall}
\end{aligned} \tag{11}$$

where $\boldsymbol{n}$ is a unit vector normal to walls.

2.3. Nanofluid properties

In this paper the nanofluid effective density ρ_{nf}, the heat capacity $(C_p)_{nf}$, and the thermal expansion coefficient (β_{nf}) are obtained by these well-known formulas [34]:

$$\rho_{nf} = (1-\varphi)\rho_f + \varphi\rho_p \tag{12}$$

$$(\rho C_p)_{nf} = (1-\varphi)(\rho C_p)_f + \varphi(\rho C_p)_p \tag{13}$$

$$(\rho\beta)_{nf} = (1-\varphi)(\rho\beta)_f + \varphi(\rho\beta)_p \tag{14}$$

where subscripts “f”, “p” and “nf” refer to fluid, particle and nanofluid, respectively.

Unfortunately, there is great ambiguity concerning the viscosity and the thermal conductivity of nanofluids. It is well accepted that these properties are influenced by many factors. Therefore, new and modified correlations for these quantities are constantly being published in the literature. By means of regression analysis of different experimental data Corcione [35] obtained empirical correlations for viscosity and thermal conductivity of nanofluids. The effect of important parameters such as temperature and particle size was considered in his formulas therefore, these correlations are frequently used in recent published papers [36–39].

Moreover, experimental results of Ghanbarpour et al. [40] confirm the validity of Corcione correlations. Therefore, these formulas are used in the present study which are as follows [35]:

$$\mu_{nf} = \mu_f\Big/\left(1 - 34.87\left(d_p\Big/d_f\right)^{-0.3}\varphi^{1.03}\right) \tag{15}$$

where d_p denote diameter of nanoparticles (given in Table 1) and d_f is the base fluid molecules diameter (for water $d_f = 0.385\ \ nm$).

$$k_{nf} = k_f\left(1 + 4.4(Re_B)^{0.4}Pr^{0.66}\left(\frac{T}{T_{fr}}\right)^{10}\left(\frac{k_p}{k_f}\right)^{0.03}\varphi^{0.66}\right) \tag{16}$$

$$Re_B = \rho_f u_B d_p\Big/\mu_f \tag{17}$$

$$u_B = 2K_B T\Big/\left(\pi\mu_f d_p^2\right) \tag{18}$$

In the above equations, T_{fr}, u_B and K_B refer to freezing point of the base fluid, nanoparticle Brownian velocity and Boltzmann's coefficient ($K_B = 1.380648 \times 10^{-23}$ J/K), respectively.

Thermo-physical properties of water and nanoparticles are summarized in Table 1.

2.4. Non-dimensional form of governing equations

The following variables are introduced to non-

Table 1
Thermo-physical properties of water and nanoparticles at T = 310 K [32].

	ρ (kg/m^3)	K (W/mK)	C_p (J/kgK)	β × 10^5 (1/K)	μ × 10^6 (kg/ms)	d_p (nm)
Al_2O_3	3970	40	765	0.85	–	33
Water	993	0.628	4178	36.2	695	–

dimensionalization of Equations (1)–(3) and (10):

$$x^* = \frac{x}{H}, y^* = \frac{y}{H}, \nabla^* = H\nabla, \boldsymbol{V}^* = \frac{\boldsymbol{V}H}{\nu_f}, p^* = \frac{pH^2}{\rho_{nf}\nu_f^2}, T^* = \frac{T - T_c}{T_h - T_c},$$
$$\varphi^* = \frac{\varphi}{\varphi_{Ave}}, D_B^* = \frac{D_B}{D_{B0}}, D_T^* = \frac{D_T}{D_{T0}}, \delta = \frac{T_c}{T_h - T_c},$$
$$Ra = \frac{g\beta_f(T_h - T_c)H^3}{\alpha_f \upsilon_f}, Pr = \frac{\nu_f}{\alpha_f} \tag{19}$$

where, $D_{T0} = \gamma \frac{\mu_f}{\rho_f}\varphi_{Ave}$, $D_{B0} = \frac{k_B T_c}{3\pi\mu_f d_p}$ and, $\alpha_f = \frac{k_f}{(\rho C_p)_f}$

Continuity equation:

$$\nabla^* \cdot \boldsymbol{V} = 0 \tag{20}$$

Momentum equation:

$$\left(\frac{\rho_{nf}}{\rho_f}\right)\boldsymbol{V}\cdot\nabla^*\boldsymbol{V} = -\left(\frac{\rho_{nf}}{\rho_f}\right)\nabla^* p^* + \nabla^*\cdot\left[\left(\frac{\mu_{nf}}{\mu_f}\right)\nabla^*\boldsymbol{V}\right] + \left[\left(\frac{(\rho\beta)_{nf}}{(\rho_f\beta_f)}\right)\cdot\frac{1}{Pr}\cdot Ra.T^*\right]\cdot\boldsymbol{e_g} \tag{21}$$

where $\boldsymbol{e_g} = \frac{\boldsymbol{g}}{|\boldsymbol{g}|}$ is a unit vector of gravitational acceleration.

Energy equation:

$$\frac{(\rho C_p)_{nf}}{(\rho_f c_{p,f})}\boldsymbol{V}\cdot\nabla^* T^* = \frac{1}{Pr}\nabla^*\cdot\left[\left(\frac{k_{nf}}{kf}\right)\nabla^* T^*\right] + \frac{1}{Pr}\cdot\frac{1}{Le}\left\{D_B^*\nabla^*\varphi^*\cdot\nabla^* T^* + \frac{D_T^*}{N_{BT}}\frac{\nabla^* T^*\cdot\nabla^* T^*}{1+\delta T^*}\right\} \tag{22}$$

Volume fraction equation:

$$\boldsymbol{V}\cdot\nabla^*\varphi^* = \frac{1}{Sc}\nabla^*\cdot\left[D_B^*\nabla^*\varphi^* + \frac{1}{N_{BT}}\cdot\frac{D_T^*}{1+\delta T^*}\nabla^* T^*\right] \tag{23}$$

In the above equations, $Sc = \frac{\nu_f}{D_{B0}}$, $N_{BT} = \frac{\varphi_{Ave}D_{B0}T_c}{D_{T0}(T_h - T_c)}$ and $Le = \frac{k_f}{\rho_p c_{p,p}\varphi_{Ave}D_{B0}}$ represent Schmidt number, diffusivity ratio parameter (Brownian diffusivity/thermophoretic diffusivity) and Lewis number, respectively [9].

The dimensionless form of boundary conditions can be written as:

$\boldsymbol{V}^* = 0$, $\nabla^* T^*\cdot\boldsymbol{n} = \nabla^*\varphi^*\cdot\boldsymbol{n} = 0$ and on the top and bottom walls.

$\boldsymbol{V}^* = 0$, $T^* = 1$ and $\nabla^*\varphi^*\cdot\boldsymbol{n} = -\frac{D_T^*}{D_B^*}\cdot\frac{1}{N_{BT}}\cdot\frac{1}{1+\delta T^*}\nabla^* T^*\cdot\boldsymbol{n}$ on the left wall.

$\boldsymbol{V}^* = 0$, $T^* = 0$ and $\nabla^*\varphi^*\cdot\boldsymbol{n} = -\frac{D_T^*}{D_B^*}\cdot\frac{1}{N_{BT}}\cdot\frac{1}{1+\delta T^*}\nabla^* T^*\cdot\boldsymbol{n}$ on the right wall.

The average Nusselt number is calculated by integrating the local Nusselt number along the hot vertical wall of cavity.

$$Nu_{Ave} = -\int\frac{k_{nf}}{k_f}\nabla^* T^*\cdot\boldsymbol{n} \tag{24}$$

2.5. Numerical method, grid study and verification

The governing equations with the associated boundary conditions are numerically solved using the SIMPLE-based finite volume method on a co-located grid [41]. diffusion terms in the governing equations are discretized using a second-order central difference scheme while an upwind scheme is used to discretize the convective terms. The thermo-physical properties such as density, viscosity and thermal conductivity as well as thermophoresis diffusion and Brownian motion coefficients, which are varied with temperature and volume fraction, are solved simultaneously with flow, temperature and volume fraction equations in the whole domain. To obtain converged solutions, under-relaxation coefficient of 0.5 is used for the momentum and the energy equations while under-relaxation factor for volume fraction transport equation is set to 0.6.

2.6. Grid study

Numerical solution of governing equations shows that there is a sharp volume fraction gradient especially near the walls; thus, the results are sensitive to the grid numbers. Fig. 2 shows the effect of grid numbers on the local nanoparticles distribution along the horizontal centerline of cavity ($y^* = y/H = 0.5$). Moreover, the average Nusselt numbers obtained using different grid numbers are presented in Table 2. From Fig. 2 and Table 2, it is seen that by changing the grid numbers from 180 × 180 to 210 × 210, the variation of nanoparticles local distribution and the average Nusselt number is not significant, thus a uniform grid system of 180 × 180 is used for all simulations.

2.7. Verification

Validation is performed for natural convection of Al_2O_3–water

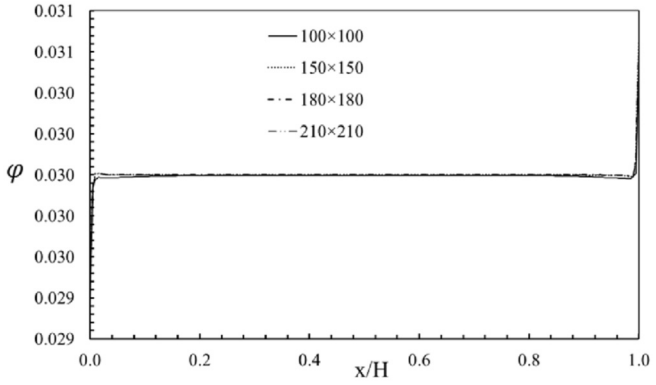

Fig. 2. Local volume fraction variation along the horizontal centerline of cavity ($y^* = 0.5$) for $Ra = 3.37 \times 10^5$, Pr=4.623, $\varphi_{Ave} = 0.03$ and $\theta = 0$.

Table 2
Effect of the grid size on the average Nusselt number ($Ra = 3.37 \times 10^5$, Pr = 4.623, $\varphi_{Ave} = 0.03$ and $\theta = 0$).

Grid	Nu_{Ave}
100 × 100	6.816478
150 × 150	6.791259
180 × 180	6.791135
210 × 210	6.791100

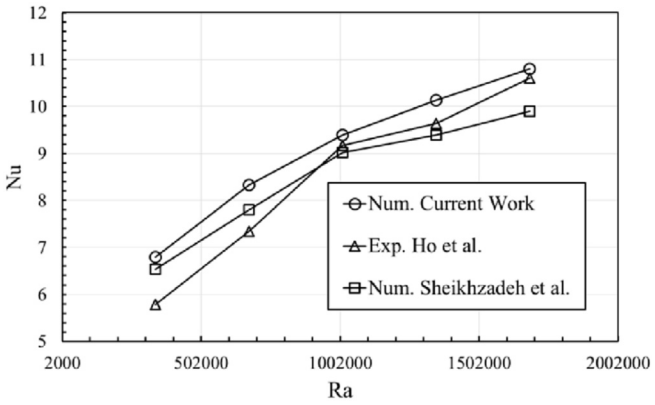

Fig. 3. Comparison of the mean Nusselt number obtained from present numerical simulation with the experimental results of Ho et al. [42] and numerical results of Sheikhzadeh et al. [13] at different Ra numbers.

nanofluid inside a square cavity for $d_p = 33$ nm, $2 \leq \Delta T \leq 10$ ($3.37 \times 10^5 \leq Ra \leq 1.68 \times 10^6$), average volume fraction of 3% ($\varphi_{Ave} = 0.03$), Pr = 4.623 and inclination angle of $\theta = 0$. Both experimental (Ho et al. [42]) and numerical results (Sheikhzadeh et al. [13] and Garoosi et al. [19]) are available for this benchmark case. It should be noted that in the above mentioned numerical studies Buongiorno's mathematical model was used. Comparison of the average *Nu* number as a function of *Ra* number is depicted in Fig. 3. In general, there is a good agreement between present results and results of [42] however; a deviation occurs between numerical results and experimental data, particularly at low Ra numbers. This is a fact that presentation a numerical model which can completely describe all hydro-thermal behaviors of nanofluids is hard, especially at high particle volume fractions. Although Buongiorno's model considers some important slip mechanisms but different and complex phenomena such as particle-particle and particle-wall collisions are absent in this formulation. Besides, the correlations of nanofluid viscosity and thermal conductivity have their own approximation. Thereby, the difference between numerical results and experimental data is somewhat acceptable. In addition, isotherms and nanoparticles distribution obtained from present work are compared with results of [13,19] in Fig. 4. As shown in Fig. 4 the present results are in close agreement with other numerical studies.

3. Results and discussion

Free convection of Al_2O_3-water nanofluid in a square cavity is simulated by using Buongiorno's two-phase model. Computations are performed at the following values of non-dimensional parameters: Rayleigh numbers ($Ra = 10^2$, $Ra = 10^4$ and $Ra = 10^6$), average particle volume fractions ($0 \leq \varphi_{Ave} \leq 0.04$), inclination angle ($0^\circ \leq \theta \leq 60^\circ$) and Lewis number ($2.62 \times 10^5 \leq Le \leq 1.05 \times 10^6$). In all cases the values of δ, Pr, Sc and N_{BT} are fixed at 155, 4.623, 3.55×10^4 and 1.1, respectively.

The effects of above mentioned parameters on flow structure,

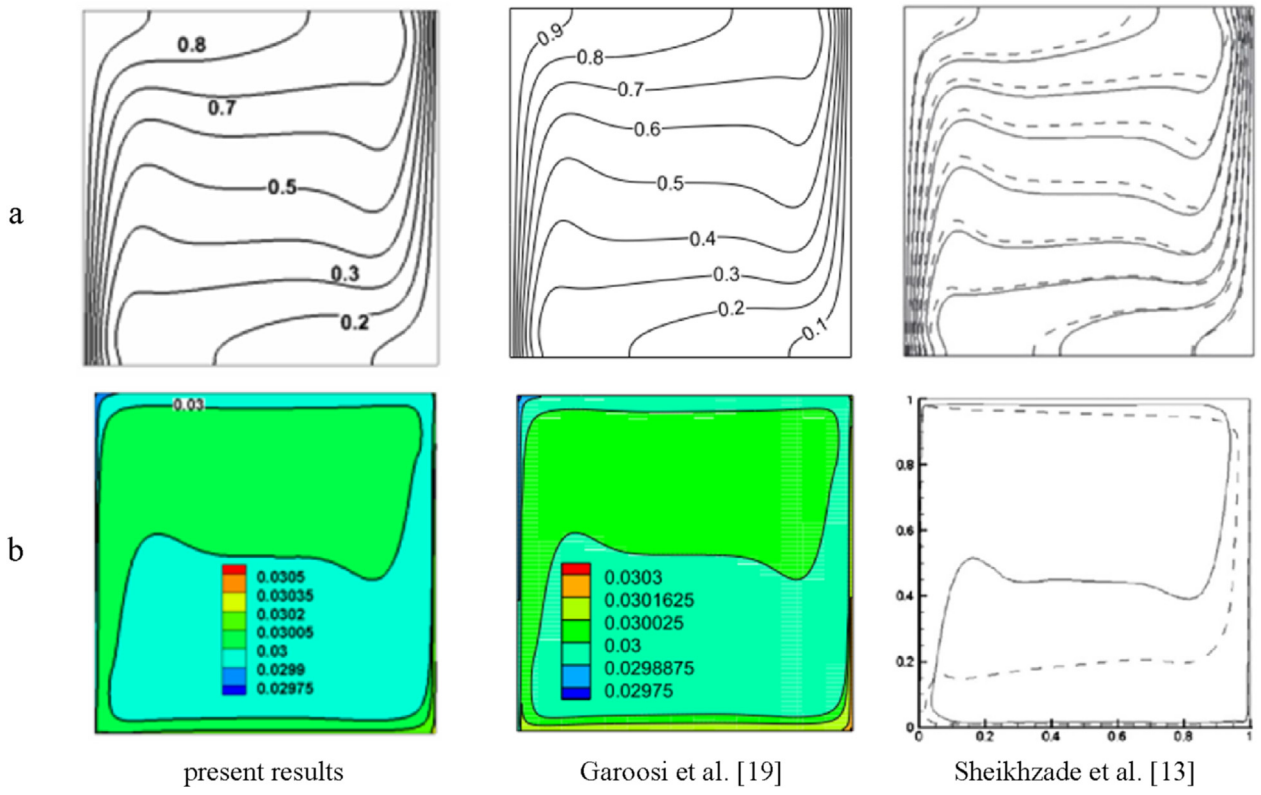

Fig. 4. Comparison of present results with the numerical results of Sheikhzade et al. [13] and Garoosi et al. [19] (a): isotherms and (b): contours of nanoparticles distribution.

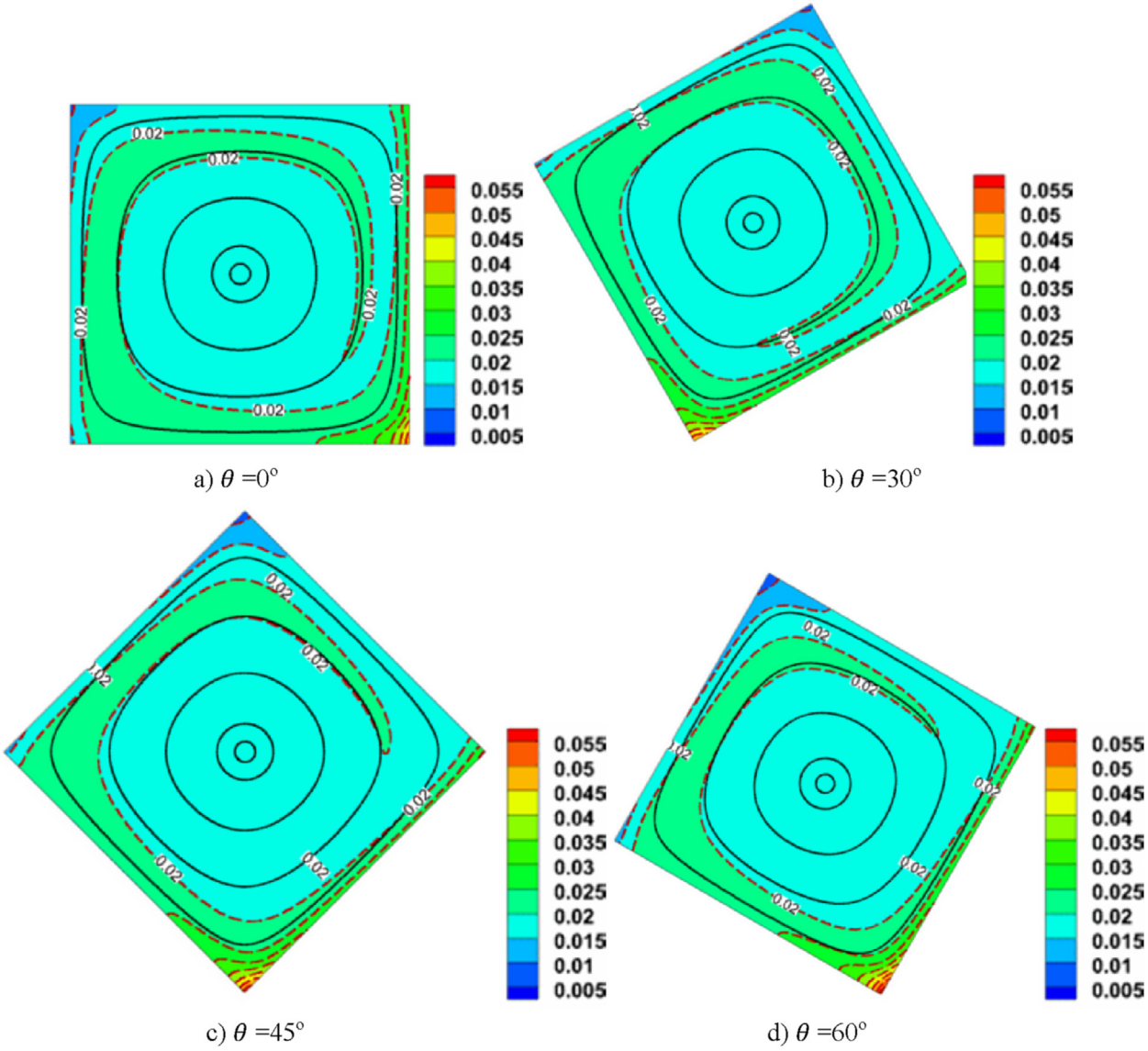

Fig. 5. Contours of nanoparticle distribution along with the constant volume fraction line of $\varphi_{Ave} = 0.02$ (red dashed line) and streamlines (solid lines) at different inclination angles for $Ra = 10^2$. (For interpretation of the references to colour in this figure legend, the reader is referred to the web version of this article.)

nanoparticle local distribution and heat transfer are presented in the following sections.

3.1. Effects of inclination angle on flow pattern and nano-particle distribution

Nano-particle distribution and streamlines for different inclination angles at two Rayleigh numbers, i.e. $Ra = 10^2$ and $Ra = 10^6$ are plotted in Figs. 5 and 6, respectively. It should be mentioned that in this section the average volume fraction is fixed at $\varphi_{Ave} = 0.02$. For better comparison, the constant volume fraction value of $\varphi_{Ave} = 0.02$ is shown by red dashed line.

The warm fluid ascends along the hot left wall and descends along the cold right wall result in formation of unicellular flow pattern at low Ra numbers. Despite decreasing buoyancy effects with increasing inclination angle, the flow pattern remains unchanged in Fig. 5. Since the buoyancy-driven flow is weak, in all inclination angles a symmetric concentric single-cell circulation is seen consistent with other published works in the literature [26,27].

Due to strong buoyancy forces at $Ra = 10^6$, the cellular flow intensifies and consequently breaks into multiple core vortex. A comparison of streamlines at $Ra = 10^2$ and $Ra = 10^6$ indicates that flow pattern near the walls are nearly the same but at $Ra = 10^6$ because of dominance of advection effects; a dumbbell-shaped flow pattern is observed. As inclination angle increases this dumbbell-shaped flow structure rotates in counter-clockwise direction.

In addition, it is seen that there is a mass boundary layer close to the vertical hot wall which grows by moving from bottom to top and on the top wall by moving from left to right. Moreover, on the cold wall another mass boundary layer exists which develops by moving from the top toward bottom and on the bottom wall by moving from right toward left. The mass boundary layers adjacent to the top and bottom walls are thinner than those close to the hot and cold walls. It can be seen that the particle concentration near the cold wall is higher than the hot wall. Thermophoretic forces are responsible for this result where temperature gradient transports

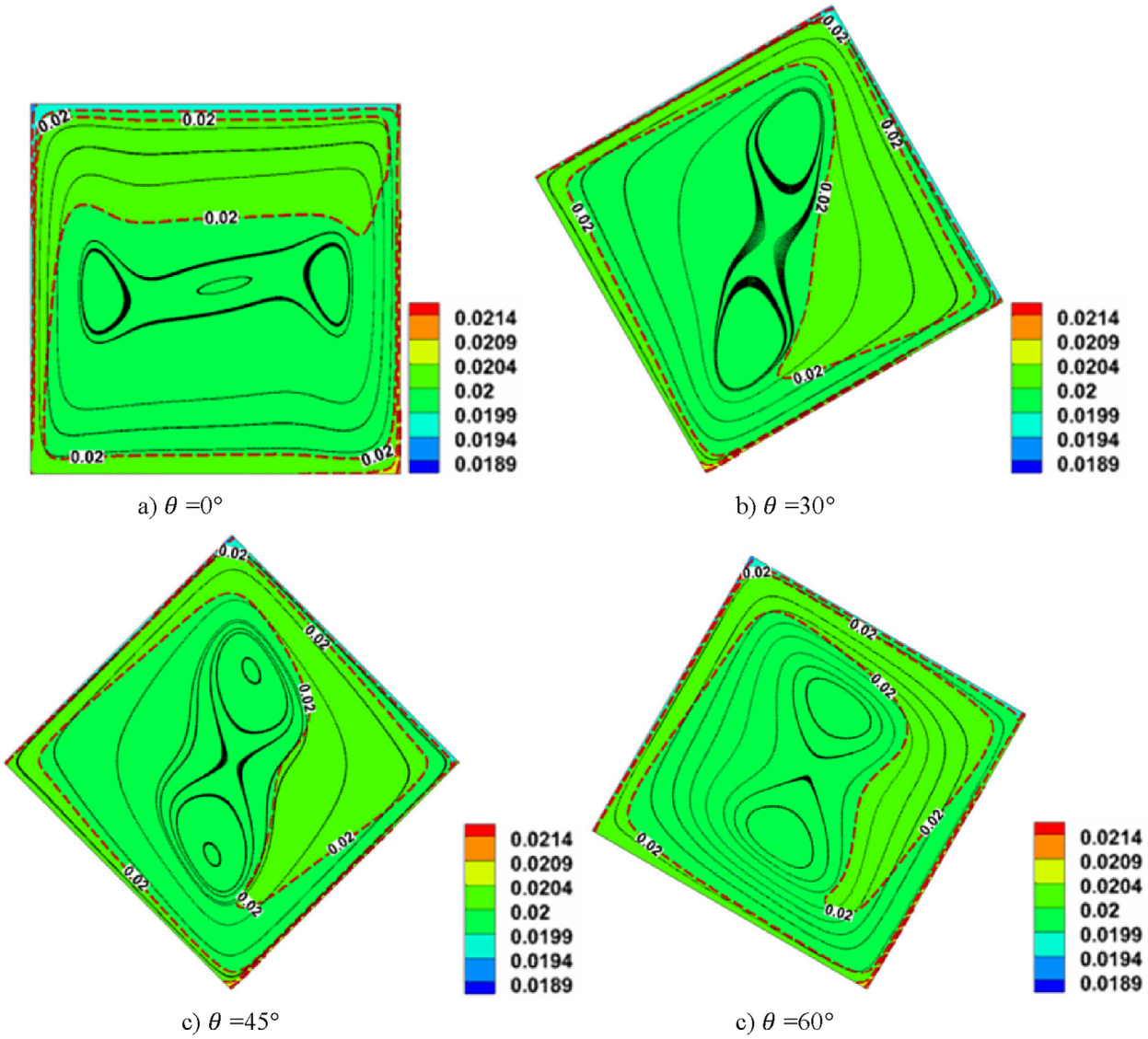

Fig. 6. Contours of nanoparticle distribution along with the constant volume fraction line of $\varphi_{Ave} = 0.02$ (dashed line) and streamlines (solid lines) at different inclination angles for $Ra = 10^6$.

the particles from hot to cold regions. Another feature of Figs. 5 and 6 is that for specified value of Ra number, as inclination angle varies from $\theta = 0^\circ$ to $\theta = 30^\circ$ the thickness of mass boundary layer grows. This is expected since with increasing θ advection effects reduce. On the other hand, for specified value of θ, with increasing Ra number the mass boundary layer thickness close to the hot and cold walls decreases.

Comparison of Figs. 5 and 6 obviously demonstrate that at $Ra = 10^2$ the nanoparticle distribution is fairly non-uniform while, at $Ra = 10^6$ it becomes nearly uniform and then homogenous models can be employed. It may be due to the fact that at high Ra numbers where advection intensifies, more particles are trapped within recirculating zones and accordingly, less deposition occurs. Similar observations were reported in Refs. [13,19].

3.2. Effects of inclination angle on temperature field

Fig. 7 shows the isotherms at different inclination angles and $Ra = 10^2$, 10^4 and 10^6.

Here the average particle volume fraction is equal to $\varphi_{Ave} = 0.02$. The uniformly distributed isotherms at $Ra = 10^2$ show that heat is primarily transferred by conduction. As shown, at this low Ra number where buoyancy-driven flow is weak, with increasing in the inclination angle the isotherms remain unchanged. Nonetheless, in higher Ra numbers ($Ra = 10^4$ and 10^6) isotherms are densely packed in the hot and cold walls. Close to the hot and cold walls, the isotherms are parallel to the walls indicating the dominance of conduction heat transfer, while in the center of the cell; convection is stronger resulting in distortion of the isotherms. With increasing Ra number from 10^4 to 10^6 the isotherms attain a more random form. In other words, as the Ra number increases, the space between the isotherms adjacent to hot and cold walls decreases further which is indicative of an increase in the heat transfer rate due to change of heat transfer mechanism from conduction to convection.

It is observed that for $Ra = 10^6$ isotherms are almost straight in central region of cavity for $\theta = 0^\circ$, meaning that there is a thermal stratification or layering and therefore, lower heat transfer rate. As inclination angle reaches $\theta = 30^\circ$, isotherms are oriented obliquely, reflecting the vigorous fluid mixing and better heat transfer rate.

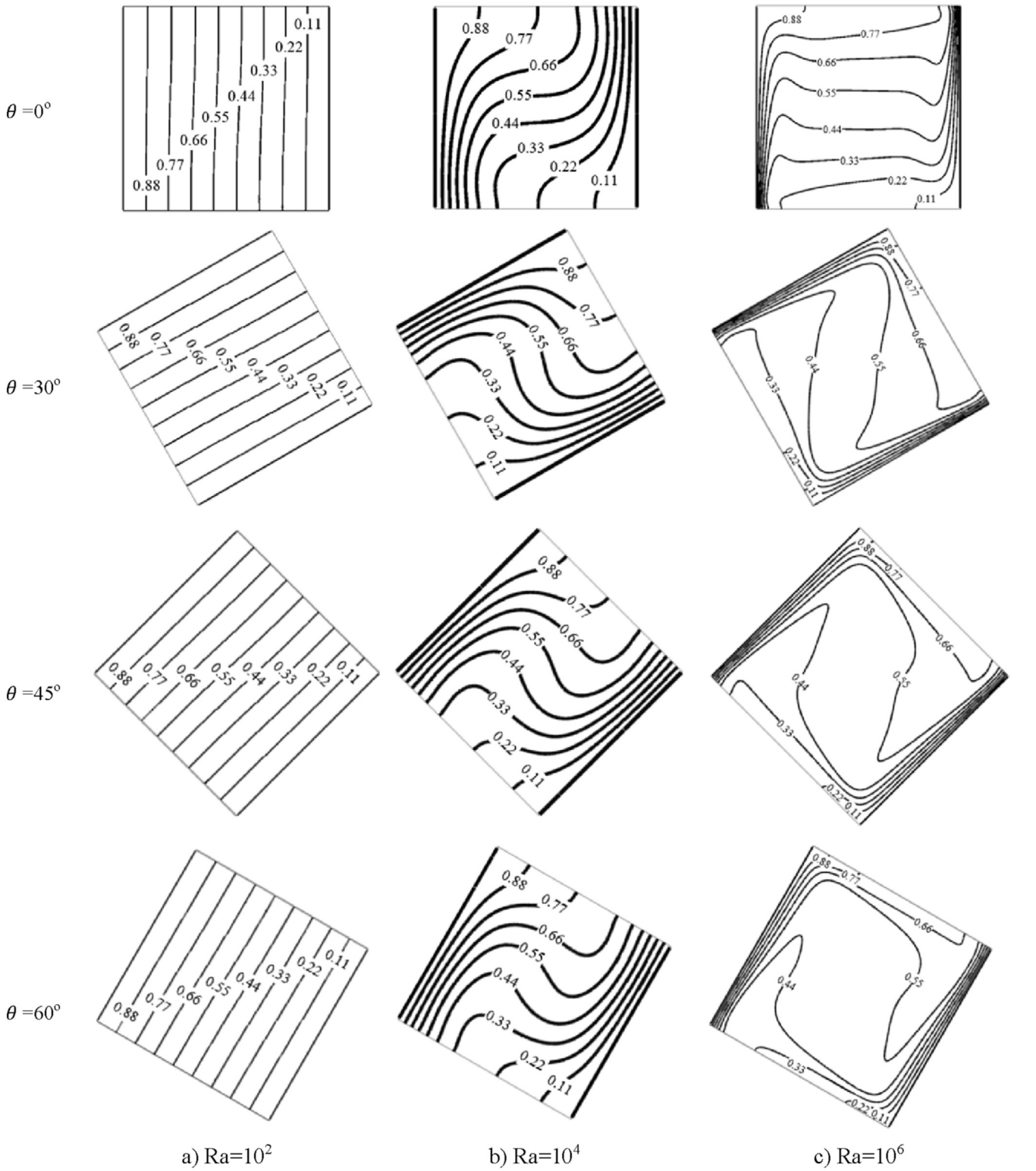

Fig. 7. Isotherms inside the cavity filled with Al2O3–water nanofluid with $\varphi_{Ave} = 0.02$ at different inclination angles and (a): Ra = 10^2 (b): Ra = 10^4 and (c): Ra = 10^6.

Above this inclination angle, isotherms again tend to become straight. The similar trend can be observed for Ra = 10^4 where the inclination angle of $\theta = 45^\circ$ leads to better mixing and higher heat transfer.

Similar qualitative observations of isotherms have been already reported in previous works based on a single-phase model, e.g., [27].

3.3. Effects of inclination angle on heat transfer rate

In Fig. 8, the variation of the average Nusselt number versus the particle volume fraction is plotted for various inclination angles and

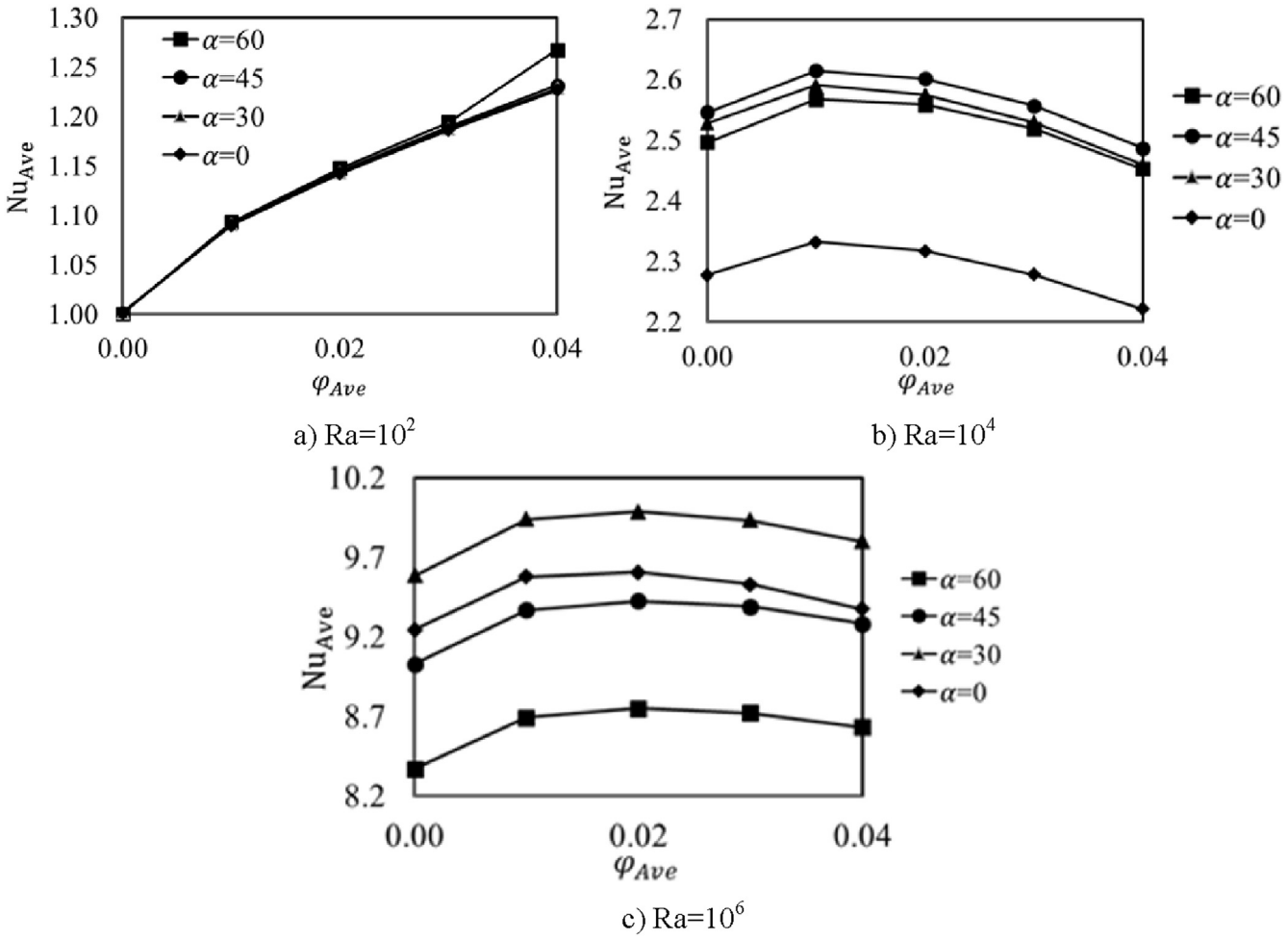

Fig. 8. Variation of the average *Nu* number versus the average particle volume fraction for various inclination angles at (a): Ra = 10^2 (b): Ra = 10^4 and (c): Ra = 10^6.

Ra numbers. The first result of Fig. 8 is that with increasing Rayleigh number, the Nusselt number rises. This is attributed to increased buoyancy forces, intense advection effects and changing flow pattern from unicellular (at Ra = 10^2 and 10^4) to multi-core vortex (at Ra = 10^6).

In addition, according to Fig. 8 at Ra = 10^2 with increasing the average volume fraction, *Nu* number rises continuously. Increasing particle volume fraction causes an enhancement in both viscosity and thermal conductivity of nanofluid. Consequently, with raising the viscosity, thermal boundary layer grows and hence the temperature gradients near the walls reduce leading to lower heat transfer rates. On the other hand, if nanoparticle volume fraction increases the thermal conductivity of nanofluid will be increased result in higher heat transfer rate. The existence of these two opposing and conflicting effects may lead to have an optimal volume fraction. As seen in Fig. 8(a), at Ra = 10^2 where conduction is the primary mechanism, *Nu* number increases with increasing φ_{Ave} but the effects of inclination angle are negligible, in accordance with results of Fig. 7. Nevertheless, for Ra = 10^4 and 10^6 it is clear that there is an optimum value of particle volume fraction (φ_{opt}) which the maximum heat transfer rate occurs. It is an interesting observation which is associated with existence of two above-mentioned competing effects. From Fig. 8, the optimum particle volume fractions are 1% and 2%, for Ra = 10^4 and 10^6, respectively. For $\varphi_{Ave} > \varphi_{opt}$, the negative effect of viscosity rise on boundary layer is stronger than the positive effects of thermal conductivity enhancement and thus heat transfer rate is decreased. Furthermore, it is evident that inclination angle has no effect on these optimum volume fraction values.

The effect of the inclination angle on the average *Nu* number for different average particle volume fractions is shown on the left hand side (LHS) of Fig. 9. It can be seen that at Ra = 10^2, which the conduction effect is dominant, inclination angle has no effect on heat transfer rate, expect φ_{Ave} = 4% where heat transfer rate increases at inclination angle of 60°. In contrast, at high Rayleigh numbers, where advection effect is strong, inclination angle affects *Nu* number at all volume fractions; with increasing the inclination angle first *Nu* number increases and reaches to its maximum value and then reduces. It is seen that regardless of particle volume fraction, the maximum *Nu* number occurs at about 45° (for Ra = 10^4) and 30° for (Ra = 10^6). This result is a consequence of isotherms orientation in central region of cavity which discussed in the previous section. The same results were obtained in Refs. [26,27,29] by single-phase modeling.

To better understanding the effect of nanoparticle volume fraction on the heat transfer enhancement, the *Nu* number variation parameter, which is defined as $\text{Nu\_Variation} = \frac{\text{Nu}_{Ave,\varphi} - \text{Nu}_{Ave,\varphi=0}}{\text{Nu}_{Ave,\varphi=0}} \times 100$, is presented on right hand side (RHS) of Fig. 9. It is found that at lowest Ra number i.e. Ra = 10^2, the minimum and maximum heat transfer enhancement correspond to about 9% (at φ_{Ave} = 0.01 in all inclination angles) and 26% (at φ_{Ave} = 0.04 and θ = 60°), respectively.

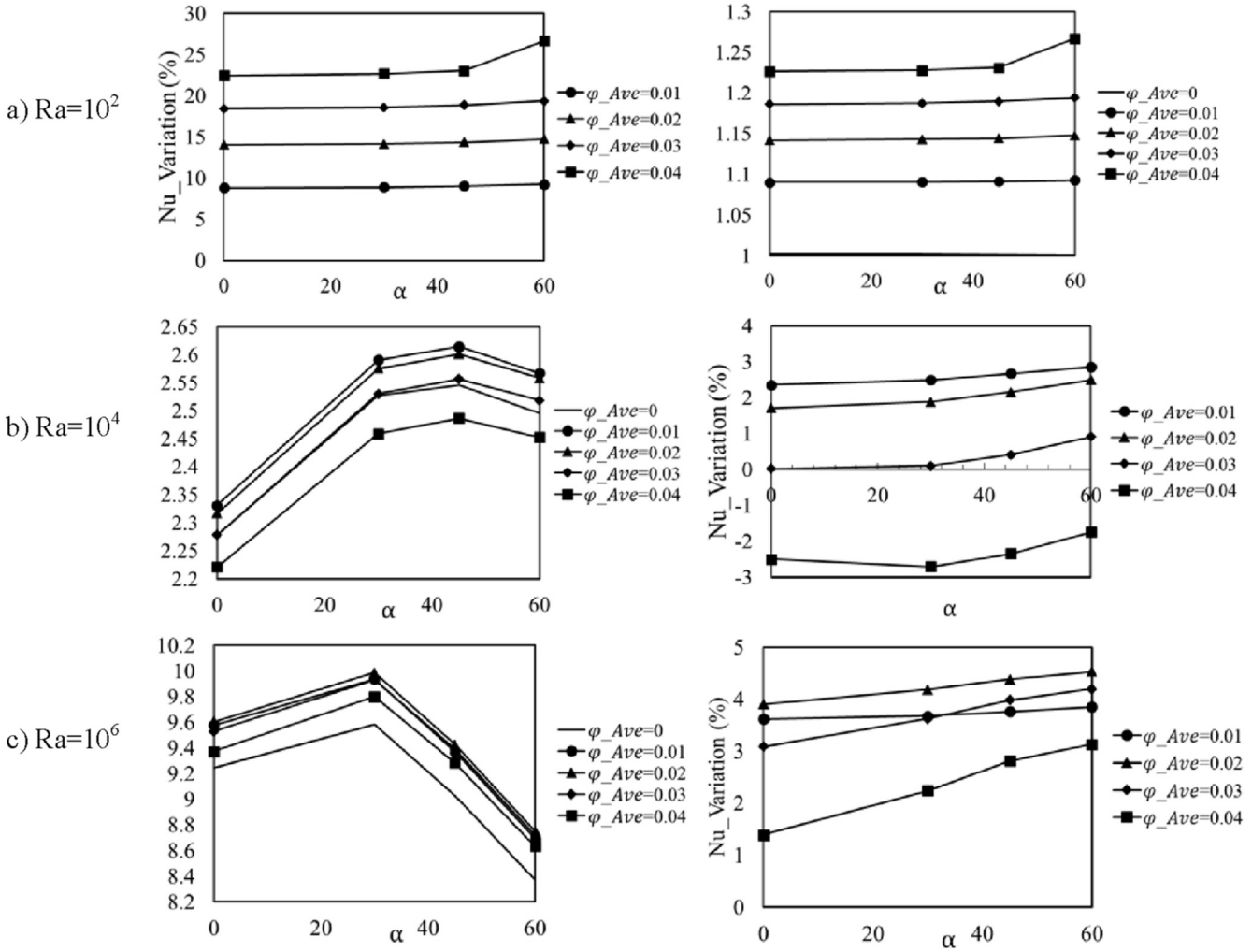

Fig. 9. *Nu* number (LHS) and *Nu* variation parameter (RHS) versus inclination angles for (a): Ra = 10^2, (b): 10^4 and (c): 10^6.

Besides, at high Ra numbers (i.e. Ra = 10^4 and 10^6) it can be seen that heat transfer enhancement at all volume fractions increases with rising of inclination angle, and reaches to its maximum value at 60°. For Ra = 10^4 and 10^6 at all inclination angles heat transfer enhancement will be minimum for the average volume fraction of 4%. At Ra = 10^4 and $\varphi_{Ave} = 0.04$, *Nu* number variation parameter has a negative value for all inclination angles indicating that heat transfer decreases by addition of nano-particles. Once again, for this volume fraction the negative effect of viscosity rise on boundary layer is stronger than positive effect of thermal conductivity augmentation. For Ra = 10^4 and 10^6 at all inclination angles heat transfer enhancement will be the maximum at the average volume fraction of 1% and 2%, respectively.

4. Conclusions

This paper studies the natural convection of Al_2O_3 water nanofluids in inclined square cavity using two phase inhomogeneous Buongiorno's model. The effects of various key parameters such as Rayleigh number ($10^2 \leq$ Ra $\leq 10^6$), volume fraction ($0 \leq \varphi_{Ave} \leq 0.04$) and inclination angle ($0^\circ \leq \theta \leq 60^\circ$) on the heat transfer rate and distribution of nanoparticles are examined. The results of this study lead to the following conclusions:

- At low Ra numbers where conduction is the dominate heat transfer mechanism regardless of inclination angle, heat transfer rate augments with increasing the average nanoparticle volume fraction of.
- At high Ra numbers where advection is strong, there are the optimal average volume fractions and inclination angles with the maximum heat transfer rate which depend on Ra number.
- At high Ra numbers, irrespective inclination angle, the particle distribution remains almost uniform. Therefore, single phase homogeneous models can be used. However, to obtain more accurate solutions and detailed physical insight two-phase models are required.
- A mass boundary layer develops along the walls of cavity. With increasing Ra number the thickness of this boundary layer reduces adjacent to hot and cold walls.

Nomenclatures

C_p	specific heat, J $kg^{-1}K^{-1}$
D_B	Brownian diffusion coefficient, kg $m^{-1}s^{-1}$
D_{B0}	reference Brownian diffusion coefficient, kg $m^{-1}s^{-1}$
d_f	diameter of the base fluid molecule, m
d_p	diameter of the nanoparticle, m
D_T	thermophoretic diffusivity coefficient, kg $m^{-1}s^{-1}$

D_{T0}	Reference thermophoretic diffusion coefficient, kg $m^{-1}s^{-1}$
g	gravitational acceleration, ms^{-2}
H	Height of cavity, m
$\boldsymbol{J}_p$	particle flux vector, kg $m^{-2}s^{-1}$
k	thermal conductivity, W $m^{-1}K^{-1}$
K_B	Boltzmann's constant = 1.38066 × 10^{-23} J K^{-1}
Le	Lewis number
N_{BT}	ratio of Brownian to thermophoretic diffusivity
Nu	Nusselt number
p	pressure, Pa
p^*	non-dimensional pressure
Pr	Prandtl number
Ra	Rayleigh number
Re_B	Brownian motion Reynolds number
T	Temperature, K
T^*	dimensionless temperature
T_{fr}	freezing point of the base fluid, K
u_B	Brownian velocity of the nanoparticle, ms^{-1}
$\boldsymbol{V}$	velocity vector, ms^{-1}
$\boldsymbol{V}^*$	normalized velocity vector, ms^{-1}
x, y	Cartesian coordinates, m
x^*, y^*	dimensionless Cartesian coordinates

Greek symbols

α	thermal diffusivity, $m^2\ s^{-1}$
β	thermal expansion coefficient, K^{-1}
δ	normalized temperature parameter
λ	constant parameter
μ	dynamic viscosity, kg $m^{-1}s^{-1}$
υ	kinematic viscosity, $m^2\ s^{-1}$
ρ	density, kg m^{-3}
φ	volume fraction
φ^*	normalized volume fraction

Subscripts

Ave	average
c	cold wall
h	hot wall
f	base fluid
p	particle
nf	nanofluid

References

[1] Maxwell JC. A treatise on electricity and magnetism. London: Clarendon Press; 1891.
[2] Choi SUS. Enhancing thermal conductivity of fluid with nanoparticles developments and applications of non-newtonian flow. ASME FED 231/MD 66. 1995. p. 99–105.
[3] Kumar DH, Patel HE, Kumar VR, Sundararajan T, Pradeep T, Das SK. Model for heat conduction in nanofluids. Phys Rev Lett 2004;93. 144301-1–;144301–4.
[4] Jayhooni SMH, Rahimpour MR. Effect of different types of nanofluids on free convection heat transfer around mini-reactor. Superlattices Microstruct 2013;58:205–17.
[5] Jmai R, Ben-Beya B, Lili T. Heat transfer and fluid flow of nanofluid-filled enclosure with two partially heated side walls and different nanoparticles. Superlattices Microstruct 2013;53:130–54.
[6] Wen D, Ding Y. Experimental investigation into convective heat transfer of nanofluids at the entrance region under laminar flow conditions. Int J Heat Mass Transf 2004;47:5181–8.
[7] He Y, Men Y, Zhao Y, Lu H, Ding Y. Numerical investigation into the convective heat transfer of TiO2 nanofluids flowing through a straight tube under the laminar flow conditions. Appl Therm Eng 2009;29:1965–72.
[8] Moghari RM, Akbarinia A, Shariat M, Talebi F, Laur R. Two phase mixed convection Al2O3 –water nanofluid flow in an annulus. Int J Multiph Flow 2011;37:585–95.
[9] Buongiorno J. Convective transport in nanofluids. J Heat Transf 2006;128:240–50.
[10] Corcione M, Cianfrini M, Quintino A. Two-phase mixture modeling of natural convection of nanofluids with temperature-dependent properties. Int J Therm Sci 2013;71:182–95.
[11] Corcione M, Habib E, Quintino A. A two-phase numerical study of buoyancy-driven convection of alumina–water nanofluids in differentially-heated horizontal annuli. Int J Heat Mass Transf 2013;65:327–38.
[12] Pakravan HA, Yaghoubi M. Analysis of nanoparticles migration on natural convective heat transfer of nanofluids. Int J Therm Sci 2013;68:79–93.
[13] Sheikhzadeh GA, Dastmalchi M, Khorasanizadeh H. Effects of nanoparticles transport mechanisms on Al2O3 –water nanofluid natural convection in a square enclosure. Int J Therm Sci 2013;66:51–62.
[14] Yadav D, Bhargava R, Agrawal GS. Numerical solution of a thermal instability problem in a rotating nanofluid layer. Int J Heat Mass Transf 2013;63:313–22.
[15] Sheikholeslami M, Ganji DD. Three dimensional heat and mass transfer in a rotating system using nanofluid. Powder Technol 2014;253:789–96.
[16] Sheikholeslami M, Gorji-Bandpy M, Soleimani S. Two phase simulation of nanofluid flow and heat transfer using heatline analysis. Int Commun Heat Mass Transf 2013;47:73–81.
[17] Tzou DY. Instability of nanofluids in natural convection. J Heat Transf 2008;72.401–130.
[18] Tzou DY. Thermal instability of nanofluids in natural convection. Int J Heat Mass Transf 2008;51:2967–79.
[19] Garoosi F, Garoosi S, Hooman K. Numerical simulation of natural convection and mixed convection of the nanofluid in a square cavity using Buongiorno model. Powder Technol 2014;268:279–92.
[20] Kakaç S, Pramuanjaroenkij A. Single-phase and two-phase treatments of convective heat transfer enhancement with nanofluids – a state-of-the-art review. Int J Therm Sci 2016;100:75–97.
[21] Vanaki Sh M, Ganesan P, Mohammed HA. Numerical study of convective heat transfer of nanofluids: a review. Renew Sustain Energy Rev 2016;54:1212–39.
[22] Ziad Saghir M, Ahadi A, Yousefi T, Farahbakhsh B. Two-phase and single phase models of flow of nanofluid in a square cavity: comparison with experimental results. Int J Therm Sci 2016;100:372–80.
[23] Sheremet MA, Groşan T, Pop I. Free convection in shallow and slender porous cavities filled by a nanofluid using Buongiorno's model. J Heat Transf 2014;136:082501.
[24] Sheremet MA, Pop I, Rahman MM. Three-dimensional natural convection in a porous enclosure filled with a nanofluid using Buongiorno's mathematical model. Int J Heat Mass Transf 2015;82:396–405.
[25] Sheremet MA, Pop I. Mixed convection in a lid-driven square cavity filled by a nanofluid: Buongiorno's mathematical model. Appl Math Comput 2015;266:792–808.
[26] Abu-Nada E, Oztop HF. Effects of inclination angle on natural convection in enclosures filled with Cu–Water nanofluid. Int J Heat Fluid Flow 2009;30:669–78.
[27] Kahveci1 K. Buoyancy driven heat transfer of nanofluids in a tilted enclosure. J Heat Transf 2010;132(6):062501–12.
[28] Aminossadati SM, Ghasemi B. Conjugate natural convection in an inclined nanofluid-filled enclosure. Int J Numer Methods Heat Fluid 2012;22(4):403–23.
[29] Ghasemi B, Aminossadati SM. Natural convection heat transfer in an inclined enclosure filled with a water-Cuo nanofluidNumerical. Heat Transf Part A Appl 2009;55:807–23.
[30] Ogut EB. Natural convection of water-based nanofluids in an inclined enclosure with a heat source. Int J Therm Sci 2009;48:2063–73.
[31] Ahmed M, Eslamian M. Numerical simulation of natural convection of a nanofluid in an inclined heated enclosure using two-phase lattice Boltzmann method: accurate effects of thermophoresis and Brownian forces. Nanoscale Res Lett 2015;10:296–308.
[32] Incropera FP, DeWitt DP. Introduction to heat transfer. New York: Wiley; 2002.
[33] McNab GS, Meisen A. Thermophoresis in liquids. J Colloid Interface Sci 1973;44:339–46.
[34] Haddad Z, Oztop HF, Abu-Nada E, Mataoui A. A review on natural convective heat transfer of nanofluids. Renew Sustain Energy Rev 2012;16:5363–78.
[35] Corcione M. Empirical correlating equations for predicting the effective thermal conductivity and dynamic viscosity of nanofluids. Energy Convers Manag 2011;52:789–93.
[36] Garoosi F, Bagheri GH, Talebi F. Numerical simulation of natural convection of nanofluids in a square cavity with several pairs of heaters and coolers (HACs) inside. Int J Heat Mass Transf 2013;67:362–76.
[37] Bianco V, Manca O, Nardini S. Entropy generation analysis of turbulent convection flow of Al2O3–water nanofluid in a circular tube subjected to constant wall heat flux. Energy Convers Manag 2014;7:306–14.
[38] Bahrehmand S, Abbassi A. Heat transfer and performance analysis of nanofluid flow in helically coiled tube heat exchangers. Chem Eng Res Des 2016;109:628–37.
[39] Garoosia F, Hoseininejad F. Numerical study of natural and mixed convection heat transfer between differentially heated cylinders in an adiabatic enclosure filled with nanofluid. J Mol Liq 2016;215:1–17.
[40] Ghanbarpour M, Bitaraf Haghigi E, Khodabandeh R. Thermal properties and rheological behavior of water based Al2O3 nanofluid as a heat transfer fluid. Exp Therm Fluid Sci 2014;53:227–35.
[41] Patankar SV. Numerical heat transfer and fluid flow. NewYork: Hemisphere Publishing Corporation; 1980.
[42] Ho CJ, Liu WK, Chang YS, Lin CC. Natural convection heat transfer of alumina-water nanofluid in vertical square enclosures: an experimental study. Int J Therm Sci 2010;49:1345–53.